Vol. 92 No. 1 pp. 74–88 ACTA GEOLOGICA SINICA (English Edition) Feb. 2018

# The Dihedral Angle and Intersection Processes of a Conjugate Strike-Slip Fault System in the Tarim Basin, NW China

WU Guanghui[1], YUAN Yajuan[1, *], HUANG Shaoying[2], Thomas Matthew Vandyk[3], XIAO Yang[1], CAI Quan[2] and LUO Bingxu[1]

1 *Guangdong Provincial Key Laboratory of Marine Resources and Coastal Engineering, School of Marine Sciences, Sun Yat-sen University, Guangzhou 510006, China*

2 *PetroChina Tarim Oilfield Company, Korla 841000, China*

3 *Department of Earth Sciences, Royal Holloway and Bedford New College, University of London, Egham, Surrey TW20 0EX, UK*

**Abstract: Recent studies, focused on dihedral angles and intersection processes, have increased understandings of conjugate fault mechanisms. We present new 3-D seismic data and microstructural core analysis in a case study of a large conjugate strike-slip fault system from the intracratonic Tarim Basin, NW China. Within our study area, "X" type NE and NW trending faults occur within Cambrian-Ordovician carbonates. The dihedral angles of these conjugate faults have narrow ranges, 19° to 62° in the Cambrian and 26° to 51° in the Ordovician, and their modes are 42° and 44° respectively. These data are significantly different from the ~60° predicted by the Coulomb fracture criterion. It is concluded that: (1) The dihedral angles of the conjugate faults were not controlled by confining pressure, which was low and associated with shallow burial; (2) As dihedral angles were not controlled by pressure they can be used to determine the shortening direction during faulting; (3) Sequential slip may have played an important role in forming conjugate fault intersections; (4) The conjugate fault system of the Tarim basin initiated as rhombic joints; these subsequently developed into sequentially active "X" type conjugate faults; followed by preferential development of the NW-trending faults; then reactivation of the NE trending faults. This intact rhombic conjugate fault system presents new insights into mechanisms of dihedral angle development, with particular relevance to intracratonic basins.**

**Key words: Conjugate fault, strike-slip, dihedral angle, fault intersection, faulting process, Carbonate**

## 1 Introduction

Conjugate faults generally have X-shaped patterns at an acute angle to the maximum compressive stress (Sylvester, 1988; Bretan et al., 1996; Nixon et al., 2011; Morley, 2014). They are especially associated with extensional regimes and occur with a variety of geometries, scales and as a result of various mechanisms (Freund, 1974; Horsfield, 1980; Sylvester, 1988; Zhao and Johnson, 1991; Nicol et al., 1995; Kelly et al., 1998; Davatzes and Aydin, 2003; Schwarz and Kilfitt, 2008; Dooley and Schreurs, 2012; Ismat et al., 2015). The initiation of conjugate faults depends on differential stress, which tends to increase with confining pressure (e.g., Thatcher and Hill, 1991; Ismat, 2015). Besides pure-shear deformation, conjugate fault deformation may be accommodated by bookshelf faulting, unidirectional extension/contraction or other non-Anderson models of deformation (e.g., Yin and Taylor, 2011). According to the Coulomb fracture criterion, the average dihedral angle of conjugate faults should be ~60°. However, in both natural and experimental settings a significant scatter in these dihedral angles has been observed and is generally attributed to variations in confining pressure (Ramsey and Chester, 2004; Ismat, 2015). Various processes may be invoked to maintain the volume balance in the intersection region of a conjugate fault pair. These include ductile thinning by inter-grain slip, pressure solution, multiple cross-cutting faulting, and mass transport toward the surface resulting in flower structures (e.g., Schwarz and Kilfitt, 2008). Convergent conjugate faults may terminate downwards by gradual decrease in displacement, detachment or volume loss (e.g., Morley, 2014).

* Corresponding author. E-mail: yuanyaj3@mail.sysu.edu.cn

In nature, conjugate strike-slip faults exist on a relatively small scale, less than hundreds of kilometers, and rarely exhibit a simple X-shaped geometry (Ferrill et al., 2009; Yin and Taylor, 2011; Morley, 2014). Most conjugate faults consist of oppositely dipping faults that intersect and cross-cut each other (Nicol et al., 1995; Ferrill et al., 2009; Morley, 2014). However the resulting intersection and cross-cutting is complicated and generally difficult to reconstruct using seismic data, easily leading to erroneous geometric interpretations (e.g., Bretan et al., 1996; Ferrill et al., 2009). Due to unstable finite-strain deformation, X-shaped geometries are relatively uncommon in intracratonic basins (Sylvester, 1988; Leithton et al., 1990; Walker et al., 2002; Dooley and Schreurs, 2012). Conjugate faults exert a range of influences of importance to hydrocarbon exploitation. These include trapping hydrocarbon accumulations, producing permeability anisotropy by preferentially enhancing or reducing permeability and reducing effective thicknesses of seal and reservoir units (e.g., Ferrill et al., 2009; Morley, 2014). However, understandings of the processes and kinematics of these faults, in the subsurface, remain limited by a lack of data.

In addition to numerous reverse faults in the Tarim basin (Jia Chengzao, 1997; Wu Guanghui et al., 2016), various strike-slip faults have been identified in recent years (Wu Guanghui et al., 2012; Lan Xiaodong et al., 2015; Sun Dong et al., 2015; Wang et al., 2016). However, there are important differences between these faults and those of other typical intracratonic basins. Using new seismic and core data, this paper presents a detailed interpretation of conjugate fault dihedral angles from the Tarim intracratonic basin. It includes discussion of the intersection of those faults, to better understand the geometry and kinematics of conjugate strike-slip fault systems.

## 2 Geological Setting

The Tarim Basin is the largest petroliferous basin in China, covering an area of $56\times10^4$ km$^2$, and is surrounded by the Tianshan, Kunlun and Altun orogenic mountains (Jia Chengzao, 1997) (Fig. 1). It is an ancient interior cratonic basin with an Archean to Early Neoproterozoic crystalline basement, overlain by thick Late Neoproterozoic to Quaternary strata (Jia Chengzao, 1997; Li Qiming et al., 2010). It records late Neoproterozoic supercontinental breakup, followed by Palaeozoic to Mesozoic opening and closure of the Tethys and finally the Cenozoic Indo-Asian collision (Jia Chengzao, 1997; Jiang Haijian et al., 2017; Li Qiming et al., 2010; Wu Guanghui et al., 2016). Today it is a complicated juxtaposition of the Palaeo- to Mesozoic intracratonic basin with a subsequent Cenozoic foreland basin (Jia Chengzao, 1997; Pang Xiongqi et al., 2010; Wang Zhe and Wang Xin, 2016; Wu Zhenhan et al., 2016).

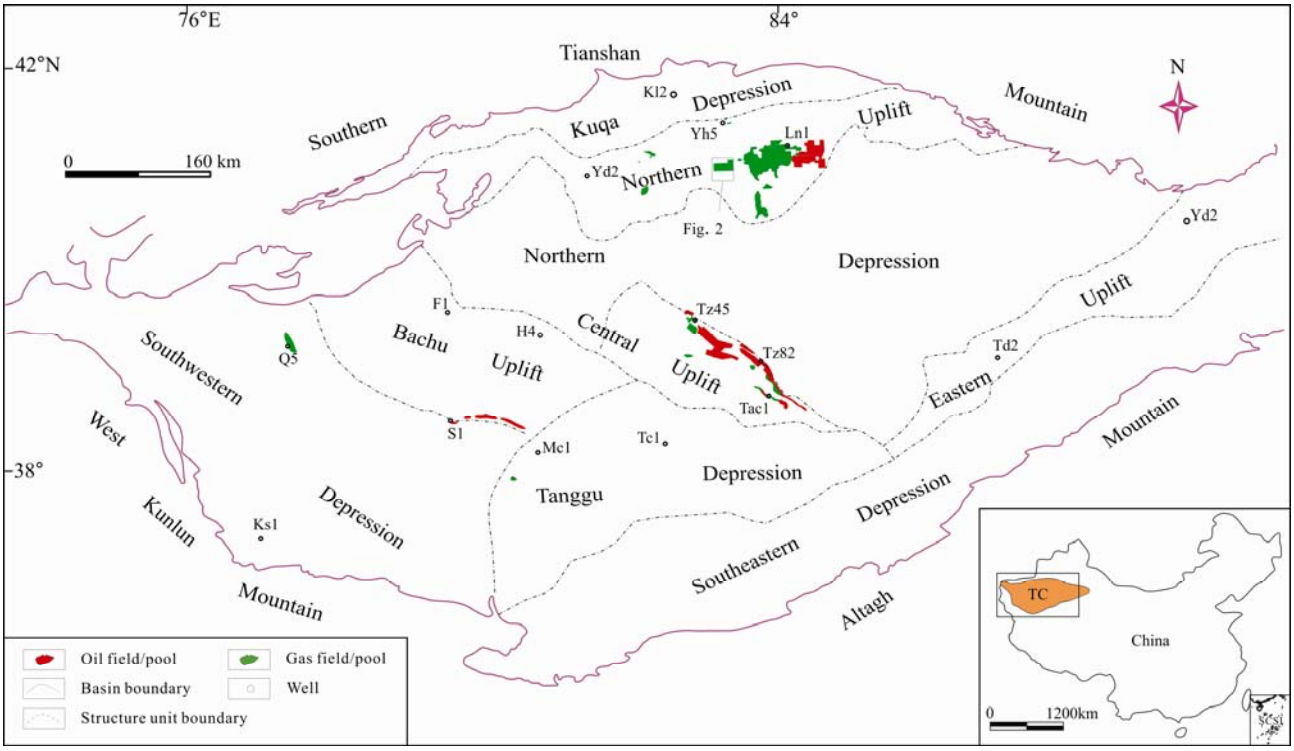


Fig. 1. The tectonic division and Ordovician carbonate oil/gas distribution in the Tarim Basin.

In recent years marine carbonates have become a significant new exploitation area in China. Both the largest carbonate oilfield and condensate field in China were discovered in the Tarim Basin (Kang Yuzhu, 2007; Du Jinhu, 2010). The region has attracted much attention, both as a new exploration frontier and as a rare example of an Early Paleozoic limestone reservoir (Jin Zhijun et al., 2009; Pang Xiongqi et al., 2010; Du Jinhu, 2010; Zhu Guangyou et al., 2013; Wu Guanghui et al., 2016). Importantly, within the Tarim Basin, most hydrocarbons are structurally trapped along fault zones (Wu Guanghui et al., 2012, 2016; Lan Xiaodong et al., 2015).

The Northern Uplift is a large Cambrian to Ordovician anticlinal uplift (Fig. 1). It is overlain by Palaeo- to Mesozoic strata, containing multiple unconformities, then thick Cenozoic deposits (Jia Chengzao, 1997; Kang Yuzhu, 2007). Multi-stage tectonic events have resulted in a complex distribution of both marine and terrestrial clastic strata (Jia Chengzao, 1997; Li Qiming et al., 2010; Wu Guanghui et al., 2016). A simplified tectonic history of the Northern Uplift can be represented by four distinct cycles (Jia Chengzao,1997; Li Qiming et al., 2010; Wu Guanghui et al., 2016): (1) A weak extensional to strong compressional stage, with a 3000 m thick carbonate platform deposited during the Cambrian to Late Ordovician, followed by Late Ordovician to Devonian fault activity (2) Stable subsidence in the Carboniferous to early Permian, followed by strong compression and uplift in the Late Permian (3) Multiple tectonic and sedimentary variations in the Mesozoic, with associated large scales unconformities (4) Rapid Cenozoic subsidence.

The Halahatang area covers around 8000 km$^2$ in the center of the southern slope of the Northern Uplift (Fig. 1). The Phanerozoic strata are relatively complete, despite a series of unconformities in the late Paleozoic to Mesozoic (Jia Chengzao, 1997; Du Jinhu, 2010). The main Cambrian to Ordovician carbonates dip gently southwards (Cui et al., 2009; Sun Dong et al., 2015), and the maximum burial depths of their uppermost strata reach 6500 - 8000 m. By contrast the overlying late Paleozoic to Cenozoic strata dip gently northwards (Cui et al., 2009; Li Qiming et al., 2010). Using high resolution 3D seismic data, X-shaped conjugate strike-slip faults have been identified in the area (Cui et al., 2009; Du Jinhu, 2010; Ni Xinfeng et al., 2013; Zhao Kuanzhi et al., 2015) (Fig. 2). Since the largest marine carbonate oilfield in China was found in the Northern Uplift of the Tarim basin (Kang Yuzhu, 2007), many further discoveries have been made around its peripheries, particularly in the Halahatang area (Du Jinhu, 2010; Zhao Kuanzhi et al., 2015). New exploitation data indicate that oil within the Halahatang area mainly occurs along fault zones, with the exception of

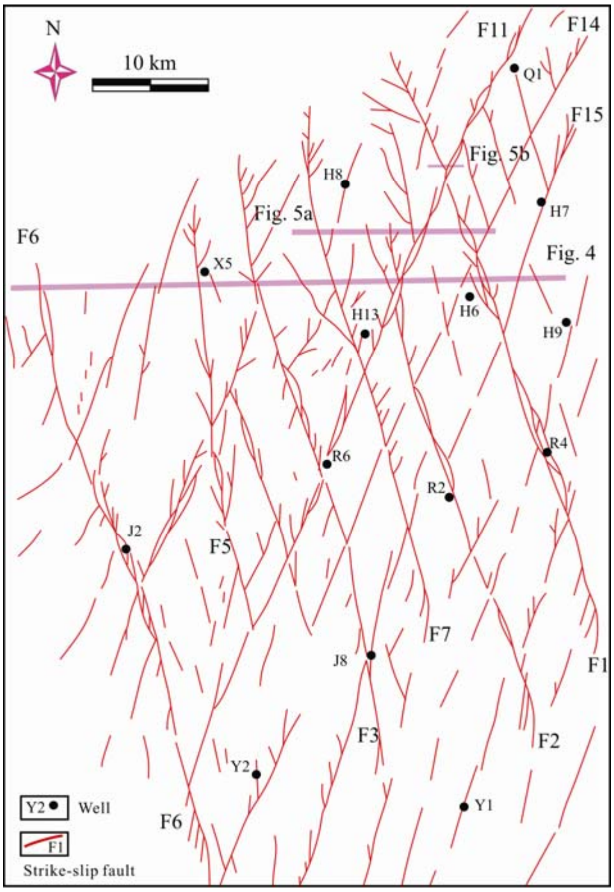


Fig. 2. The strike-slip fault system of the Ordovician carbonate in the Halahatang area.

the northeastern oilfield where it is associated with the unconformity on the top of the Ordovician carbonate rocks (Kang Yuzhu, 2007; Jin Zhijun et al., 2009; Zhu Guangyou et al., 2013). Importantly most of Halahatang Oilfield occurs at depths greater than 7000 m and has travelled southwards into the Northern Depression, with approximately 1 million t/y productions from the complicated carbonate reservoirs. Nevertheless, the related fault processes and their evolution remain poorly understood (Du Jinhu, 2010; Wu Guanghui et al., 2016).

## 3 Data and Methods

Since 2007, new data acquisition and processing techniques have produced an abundance of high resolution 3-D seismic data from the Taklimakan desert (Cui et al., 2009; Zhao Kuanzhi et al., 2015). In the Halahatang area more than 6000 km$^2$ of superdeep carbonates have been seismically surveyed. Prestack depth migration seismic data cover almost the entire Halahatang area, allowing for detailed structural analysis and reservoir description (Cui et al., 2009; Peng Gengxin et al., 2011; Zhao Kuanzhi et al., 2015).

Aided by well calibration, the main horizon strata are easily identified in seismic profiles of the slope. In addition to marker horizon offset, larger strike-slip faults may by identified by offsets of high-dip seismic reflectors. Flower structures and abrupt changes of the upthrown side or dip are also useful in identifying strike-slip faults (Cui et al., 2009; Wang Hui and Liu Mian, 2013; Sun Dong et al., 2015). Due to limited seismic resolution in the superdeep basin, small-displacement faults may show relatively continuous reflection or a kink-shape in seismic profiles. However, certain seismic attributes are useful in the identification of small faults (Peng Gengxin et al., 2011; Sun Dong et al., 2015) (Fig. 3). Seismic, particularly coherence, data are used to identify localized offsets of the anticline, lithofacies or palaeo-channels. These in turn are used to interpret fault distribution and horizontal separation. The combination of seismic attributes and profile analysis has allowed high resolution fault interpretation and structural mapping in the Halahatang area. The interpretation of these faults is aimed at guiding well-deployment and has been tested by the drilling of over 100 wells (Sun Dong et al., 2015; Wu Guanghui et al., 2016).

Using our fault interpretation and structural mapping we collated fault orientation, length and along-strike throw to elucidate fault geometries and kinematics. Since displacements are small, unclear and influenced by fold drag in seismic profiles, we used the height difference between the peak or bottom of the fault zone and the top of the Ordovician carbonate host rocks as a means of displacement analysis (Wu Guanghui et al., 2016). At the hand specimen to microscopic scale we analysed fractures in core and thin section. Synthesizing the above data, we herein present a discussion of the factors controlling both the dihedral angles of the conjugate fault systems and the accompanying processes of fault intersection in the Halahatang area.

## 4 The Geometry of the Strike-slip Fault System

### 4.1 Typical fault styles

In seismic profiles of the Halahatang area, strike-slip faults within the Lower Paleozoic strata generally exhibit positive flower structures and vertical sole faults. By contrast those within Upper Paleozoic to Mesozoic strata exhibit negative and half flower structures (Figs. 4 and 5).

Small faults commonly have a nearly vertical slip surface (dip > 85°) with a small displacement (Fig. 4). In convergent fault zones, within the Ordovician strata, positive flower structures are well developed (Figs. 4 and 5a). Some fault branches grow upward along the main

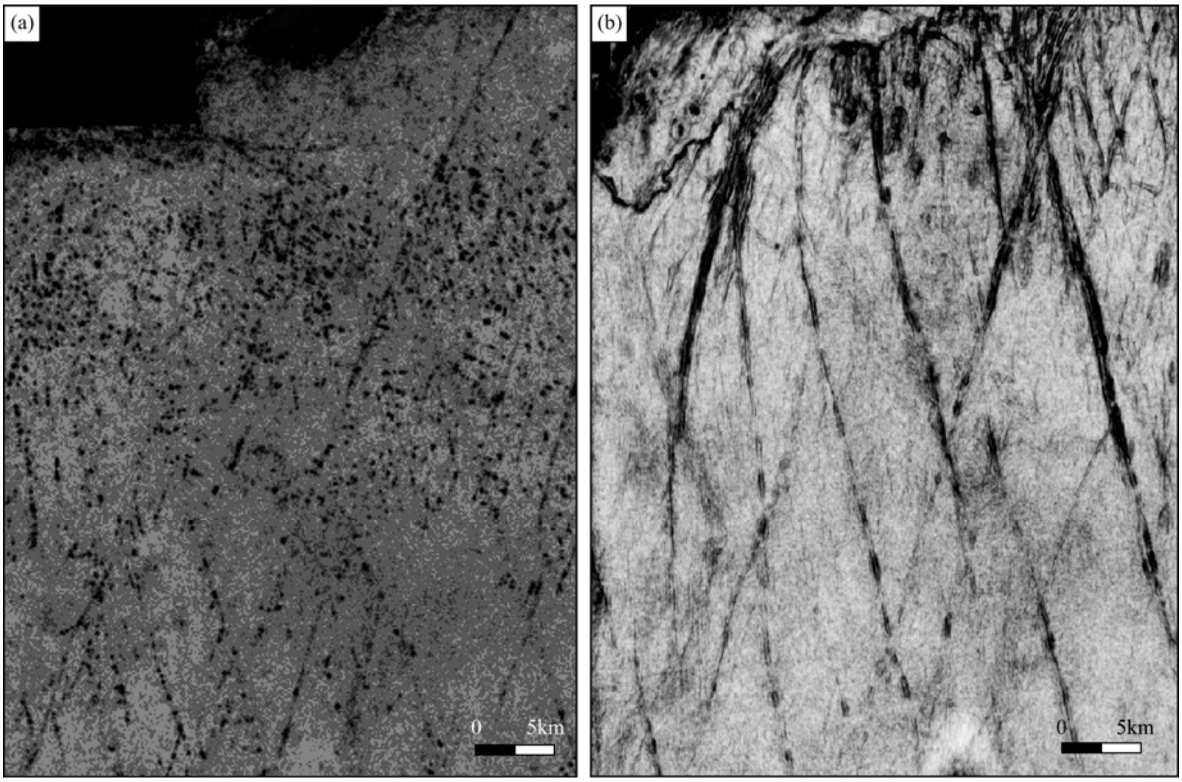


Fig. 3. The coherence cube on the top of Ordovician carbonate (a) and the top of Lower Cambrian (b) showing fault traces in the Halahatang area.
The dark continuous lines indicate fault traces, and the dark dots are possibly images of caves.

trunk to define fault horsts. These faults steepen with depth, converge and merge downward into fault trunks (Harding, 1990). Positive flower structures often vary laterally and sometimes transition to transtensional fault segments. Negative flower structures also steepen with depth, however their branches generally grow into the Permian or Cretaceous strata and have larger downward displacements (Fig. 5a). They may have two or more branches that spread upwards to define small downthrown blocks within a wider damage zone. There is typically a variation in displacement along these fault zones and some fault branches only develop on one side of the fault zone, forming half flower structures (Fig. 4).

The tips of strike-slip faults in the Halahatang area tend to develop horsetail or pinnate structures (Sun Dong et al., 2015), characterized by a series of divergent branch faults from the trunk (Fig. 2). The tips of these primary faults may also be accompanied by en echelon oblique-arranged faults of a transpressional character, which are associated with complicated fault blocks in Ordovician strata. The displacement of primary faults decreases as the splay displacement of associated horsetail or pinnate structures

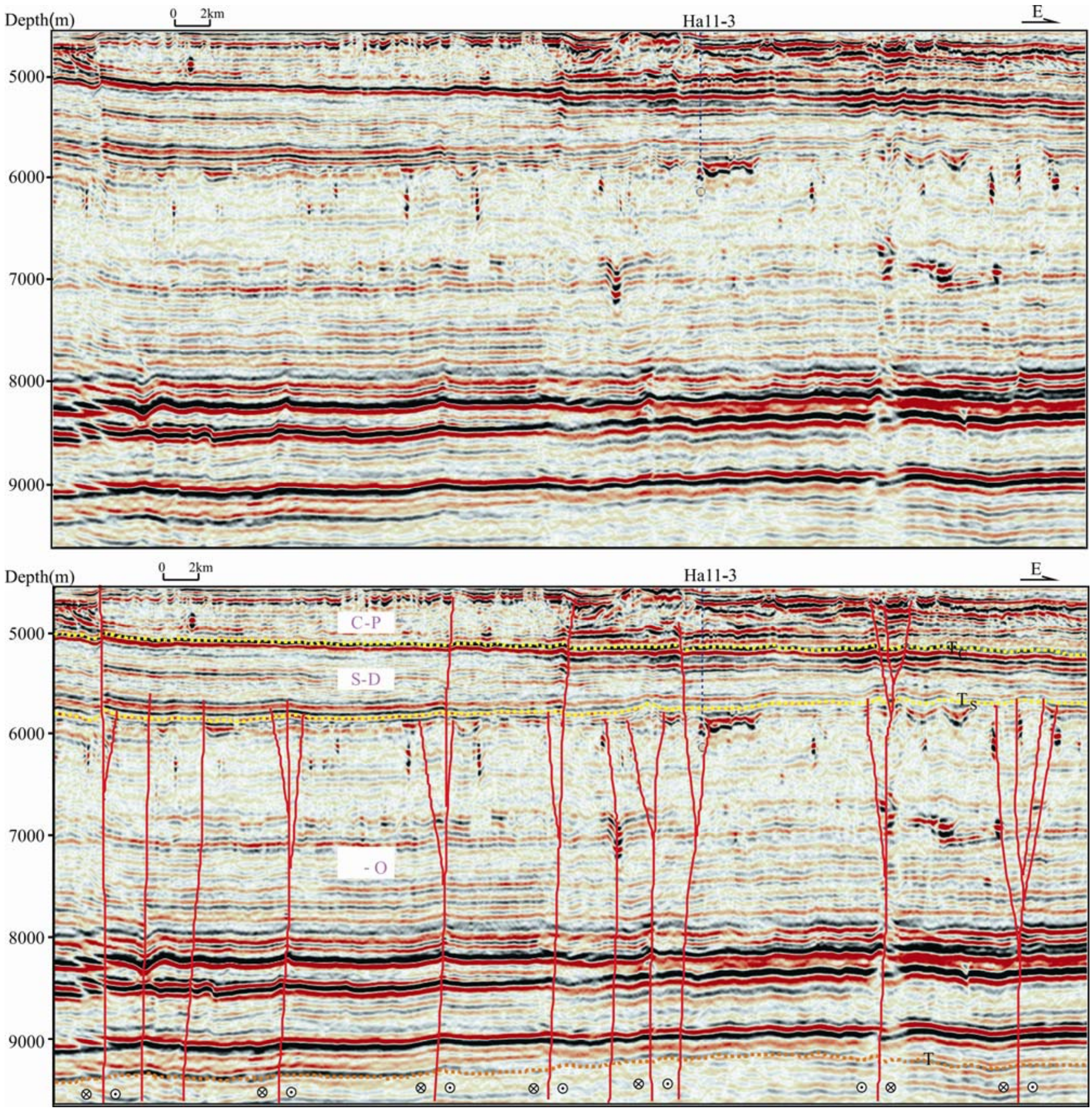


Fig. 4. The typical strike-slip fault in uninterpreted (a) and interpreted (b) seismic profiles in Halahatang area.

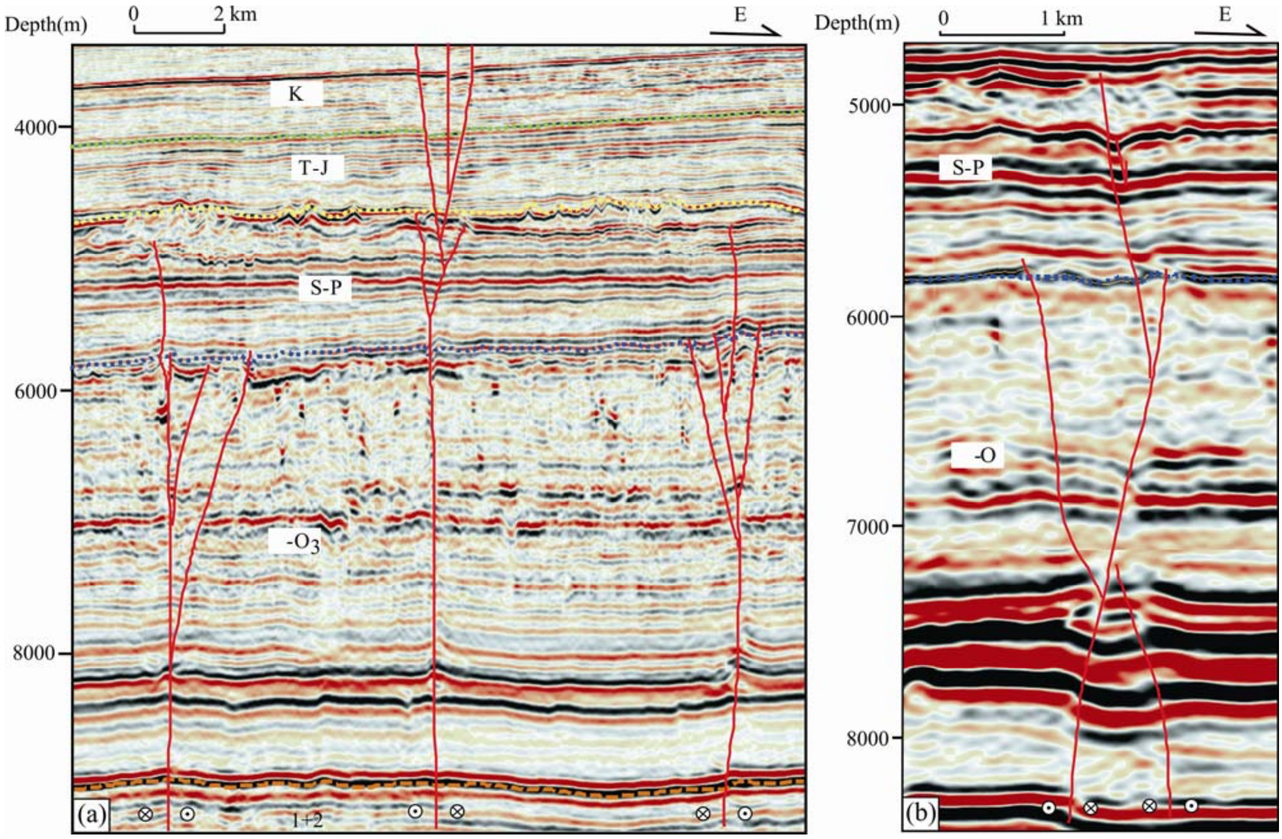


Fig. 5. A typical profile showing multi-layer strike-slip fault (a) and intersection of conjugate faults (b).

increases. By contrast, as fault zones widen these splay displacements tend to decrease. Within horsetail structures primary faults have a small displacement and steep slip surface, whereas their splays gently dip but steepen as the fault zone widens.

### 4.2 Fault distribution

According to regional structural interpretations and fault mapping, strike-slip faults in the Halahatang area were mainly developed in three structural layers: Cambrian to Ordovician, Silurian to Permian and Mesozoic (Figs. 2–5). Most of these strike-slip faults occur in the Lower Paleozoic. However, some of the major faults grew up to the Permian, or even the Cretaceous, through fault inheritance and reactivation. As a result, layers of different flower structures are stacked upon one another (Fig. 4). Specifically, positive flower structures characterise the Lower Palaeozoic strata, whereas negative flower structures occur in the overlying Permian to Mesozoic strata (Figs. 4 and 5).

Strike-slip faults, of various structural types, are widely distributed in the Ordovician carbonates (Figs. 2–5). By combining structural mapping and coherence data, we have identified a fault system consisting of symmetrical "X" type conjugate faults in plan view (Fig. 2). NE and NW strike slip faults truncate each other, generally involving a sinistral fault cutting across a dextral fault to produce a small included angle (Fig. 5b). At the conjugate fault intersection there is a wide damage zone and both of the conjugate faults are associated with positive flower structures of similar scales. These "X" shear faults, within lower Palaeozoic strata, have a very small vertical throw (< 140 m) in comparison to their length (≤ 70 km). The NW-SE and NE-SW trending faults spread across the area and impose a rhombic pattern upon the Ordovician carbonates. The linking of the resulting fault segments forms large linear fault zones accompanied by multiple secondary faults.

The Silurian to Permian strata mostly consist of linear structures or half flower structures. These are inherited from and merge downward into trunk faults. Transtensional faults, which contrast to the transpressional faults of underlying strata, indicate a change in stress field associated with a new stage of fault activity. This change is further supported by juvenile grabens superimposed upon lower horsts by fault inversion (Fig. 5a). Branch faults reach down to join trunk faults in the Cambrian to Ordovician strata. Strike-slip faults in the Mesozoic are concentrated in several major NE-SW trending fault zones. In association with stronger transtension, a series of *en echelon* structures has developed from the roots of these faults and spread upwards to form micro-grabens

(Figs. 4 and 5a). Where these faults merge down to the main Cambrian to Ordovician fault zone they cut across and remodify lower blocks.

### 4.3 Fault parameters

Fault interpretation and mapping show that sets of conjugate strike-slip faults within the Ordovician strata form an "X" type intersection in plan view (Fig. 2). The constituent conjugate faults strike NW-SE and NE-SW. The NW-SE faults are better developed than the NE-SW. They are mostly right-lateral and strike from ∠330° to ∠360° (Fig. 6a), producing sub-parallel faults. The poorer developed NE-SW faults strike from ∠16° to∠30° and are left-lateral. They become less continuous towards the southwest and are best developed in the northeast corner.

The intersection angles between major conjugate faults at the top of the Ordovician carbonates range from 26.3° to 51.1°, with a mean of 39.9° and mode of ~44° (Fig. 6b). At the base of the Cambrian carbonates there are fewer secondary faults than in the upper layers (Figs. 2–5). Here the conjugate faults have a larger range of dihedral angles, 19° to 62.3°. However, their mean is 39° and mode ~42° (Fig. 6c), which are both consistent with the Ordovician data. Compared with other areas (e.g., Ferrill et al., 2009; Ismat, 2015) the scatter of dihedral angles in the Halahatang area is small, hence the conjugate fault system forms a well-developed rhombic shape (Fig. 2). There are several significant deviations from the modal dihedral angle but these are attributable to small, irregular, unmatured faults. According to the Coulomb fracture criterion (e.g., Ismat, 2015), the average dihedral angle of a conjugate-fault should be ~60°. However, both mean and mode angles in the Ordovician and Cambrian carbonates of the Halahatang area are significantly less than this.

The secondary fault orientations are highly variable and their intersection angles with major faults vary considerably, from 6° to 71° (Fig. 6d). Most secondary faults are R shear with positive angles. Some symmetric antithetic P shear faults display negative intersection angles with the major faults, but few R' shears have developed in the area. Most of the intersection angles between secondary and primary faults have angles lower than 60° and their mode is ~40°, which is lower than the

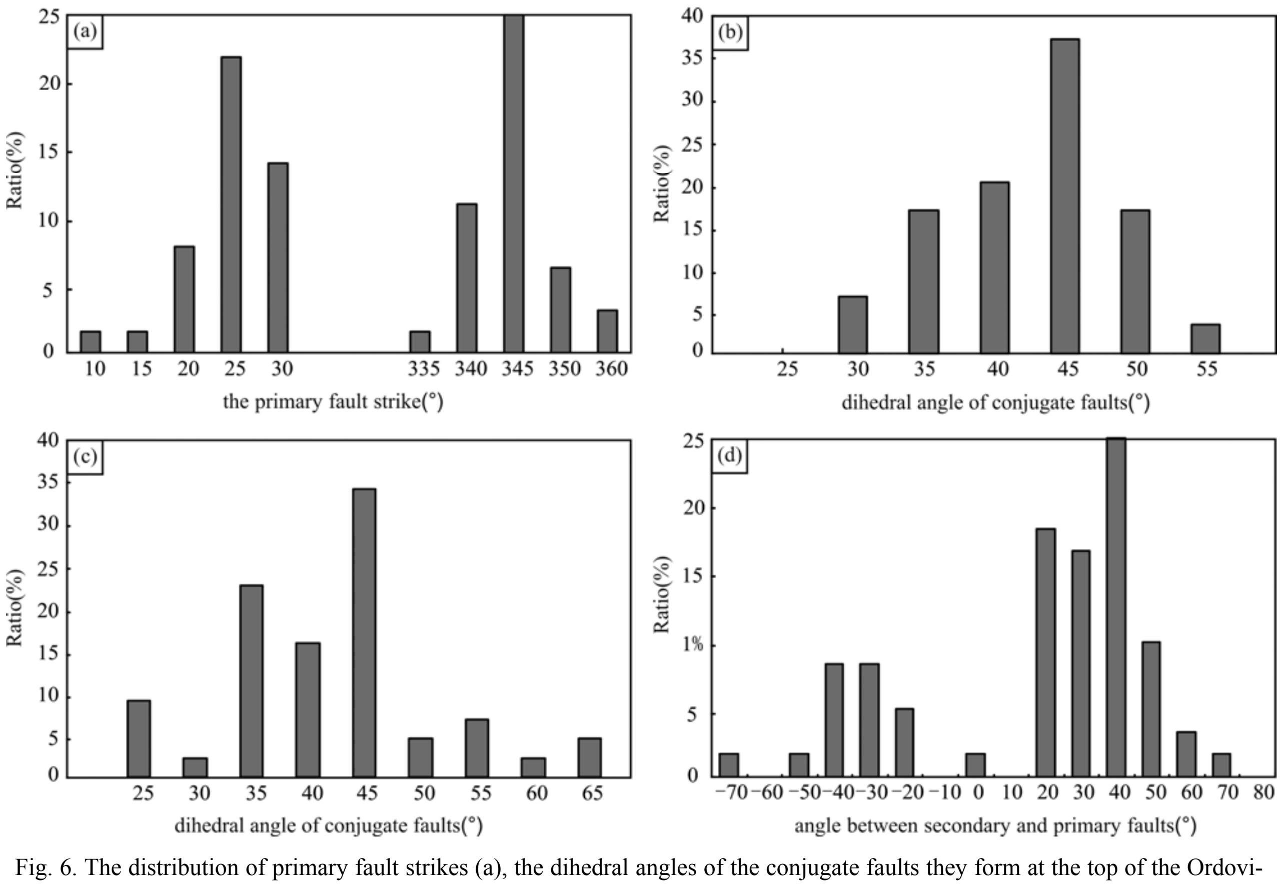


Fig. 6. The distribution of primary fault strikes (a), the dihedral angles of the conjugate faults they form at the top of the Ordovician carbonates (b), on the bottom of the Cambrian carbonate (c) and the angle between secondary and primary faults (d).
Positive angles are between the synthetic secondary fault and primary fault, and negative angles are between the antithetic secondary fault and primary fault.

modal dihedral angle between conjugate major faults. There is some correlation between the strike of secondary faults and the angle they form with major faults.

The dihedral angles of the conjugate faults show a strong negative correlation with the strike of NW-SE trending faults, but a weak positive correlation with the strike of NE-SW trending faults (Figs. 7a, 7b; Table1). This suggests the dihedral angles are related to the orientation of the NW trending faults more than to the NE trending faults. Taken together, except for a few scattered data mostly attributable to small irregular faults, conjugate fault dihedral angles demonstrate a good correlation with the orientation of major faults. This suggests major fault orientation is a controlling factor on dihedral angles.

By mapping faults using 3-D seismic data we can effectively measure their length, yet it is hard to accurately ascertain horizontal separations. Therefore, vertical height difference (throw) measured in seismic sections is the preferred method of determining displacement in these faults (Wu Guanghui et al., 2016). The length of primary faults was found to be around 5 to 60 km (Fig. 8a) and secondary faults 2 to 15 km. Resolving faults of less than 4 km was however problematic, given the resolution of available seismic data. The ratio of fault displacement to fault length in primary faults is very small, with vertical throw less than 140 m (Fig. 8b) and varies greatly along strike. Note that the NW trending faults (e.g. F1 in Fig. 8b) generally have larger vertical throws than the NE trending faults (e.g., F11 in Fig. 8b). This suggests that block movement in the intersection area depends more on the NW than the NE trending faults.

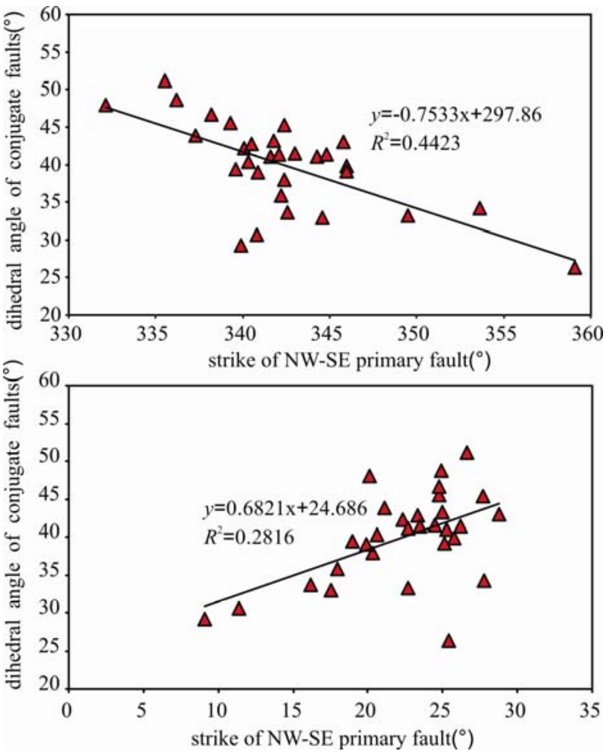


Fig. 7. Dihedral angles vs. NW trending faults (a) and NE trending faults (b) at the top of the Ordovician carbonate in the Halahatang area.

### 4.4 Microstructures in fault zones

Through observation of fractures in core, thin section

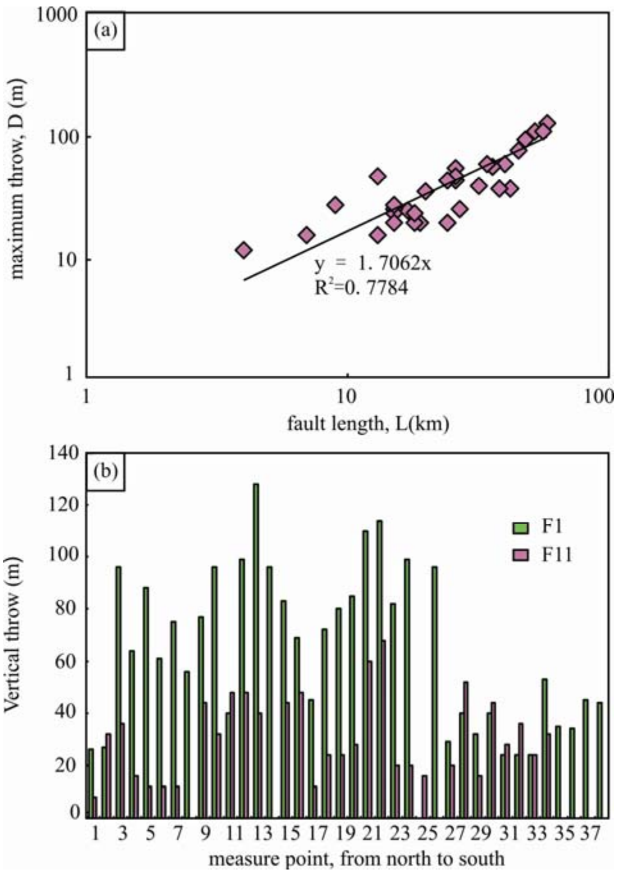


Fig. 8. Length of primary faults versus their maximum throws in the Halahatang area.

**Table 1 The dihedral angles vs. faults at the top of the Ordovician carbonate in Halahatang area**

| Angle (°) | | Value | | | | | | | | | | | |
|---|---|---|---|---|---|---|---|---|---|---|---|---|---|
| azimuth angle | NW | 340.1 | 337.3 | 342.4 | 339.6 | 345.8 | 339.3 | 339.9 | 342.6 | 340.8 | 338.2 | 344.3 | 342.4 |
| | NE | 22.3 | 21.1 | 27.7 | 19 | 28.8 | 24.8 | 9.1 | 16.2 | 11.4 | 24.8 | 25.3 | 20.3 |
| dihedral angle | | 42.2 | 43.8 | 45.3 | 39.4 | 43 | 45.5 | 29.2 | 33.6 | 30.6 | 46.6 | 41 | 37.9 |
| azimuth angle | NW | 343 | 335.5 | 349.5 | 344.6 | 340.3 | 346 | 346 | 344.8 | 340.5 | 353.6 | 359.1 | 336.2 |
| | NE | 24.5 | 26.6 | 22.7 | 17.5 | 20.6 | 25.8 | 25.1 | 26.2 | 23.3 | 27.8 | 25.4 | 24.9 |
| dihedral angle | | 41.5 | 51.1 | 33.2 | 32.9 | 40.3 | 39.8 | 39.1 | 41.4 | 42.8 | 34.2 | 26.3 | 48.7 |
| azimuth angle | NW | 332.1 | 341.6 | 342.1 | 340.9 | 341.8 | | | | | | | |
| | NE | 20.1 | 22.7 | 23.5 | 19.9 | 25 | | | | | | | |
| dihedral angle | | 48 | 41.1 | 41.4 | 39 | 43.2 | | | | | | | |

and FMI photographs (micro-resistivity image logging) we identified a number of different multi-stage fracture types in the Ordovician carbonates (Fig. 9). In both core and thin section, obliquely-arranged, *en echelon* and conjugate fractures occur in many wells (Figs. 9a, 9b, 9c). These include bifurcating splays with small intersection angles (Fig. 9b) and complicated conjugate fracture networks with a variety of intersection angles (Fig. 9c). The latter sometimes result in breccia development in fault damage zones. In thin section, conjugate fractures are common and have complicated intersection relationships. Their intersection angles are mostly less than 60°, although some have greater angles than the large-scale conjugate faults. These conjugate fractures may offset or cross-cut each other or they are cross-cut by later fractures. Some fractures terminate in another conjugate fracture, with secondary fractures developing in the confluent intersection area (Figs. 9d–9e).

There have been multiple stages of diagenesis within the Ordovician carbonates (Du Jinhu, 2010). In both core and thin section between two and four generations of calcite cement were observed in fractures (Fig. 9). Early cements are often finely crystalline where they line fracture walls, but coarsely crystalline in the centre of fractures. Some cement filled fractures have reactivated along their previous trace, suggesting two to four periods of fracture activity. Fluid inclusion analysis indicates that there have been multiple phases of fluid activity within the fractures (Zhu Guangyou et al., 2013). In many wells, fracture reactivation has resulted in the widening of pre-existing fractures (Fig. 9).

## 5 Discussion

### 5.1 The dihedral angle of conjugate-faults

In global terms, both experimental and field data reveal a significant scatter in the average value of conjugate-fault dihedral angles (Mandl, 2000; Ismat, 2015). This deviation from the 60° angle predicted by the Coulomb fracture criterion is also true of the Ordovician carbonates we report herein. In detail these dihedral angles range from 26° to 51°, with a mode of 44° and mean of 40° (Fig. 6b). Previous studies have suggested that confining pressure is the main controlling factor of this deviation. Specifically, that conjugate fault dihedral angles increase with increasing confining pressure (Ramsey and Chester, 2004; Ismat, 2015). Therefore, in theory, the dihedral angles observed in the Halahatang area may be used as a proxy for confining pressure and hence depth at the time of deformation (e.g., Ismat, 2015).

Despite today's deep burial of the Lower Paleozoic strata of the Halahatang area (Fig. 4) (Sun Dong et al., 2015; Wu Guanghui et al., 2016), faulting of the Ordovician carbonates is thought to have occurred when its top was only 1000 m deep (Cui et al., 2009; Zhu Guangyou et al., 2013). Even if the last fault activity of these Ordovician strata continued into the Mesozoic, the depth would still have been less than 2500 m. Ismat

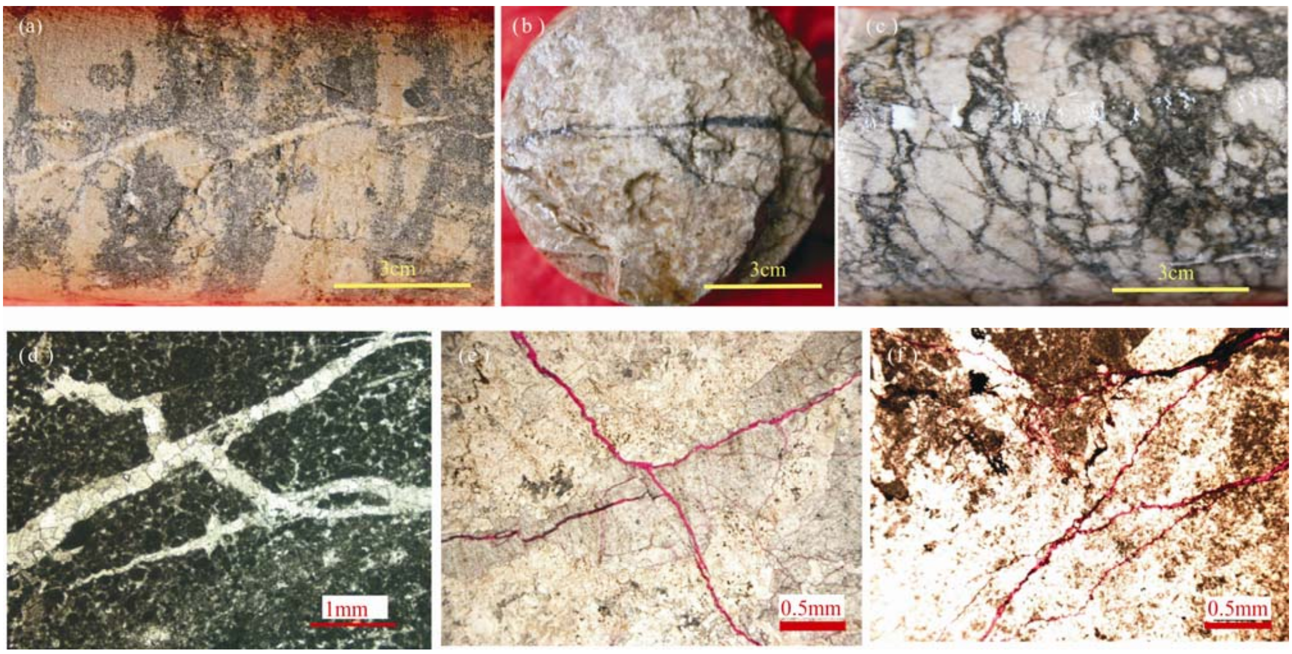


Fig. 9. Photographs of fractures from core (a-c) and thin section (d-f) of the Ordovician strata of the Halahatang area.
Porosity has been impregnated with a pink dye resin. (a) En echelon tension fractures with calcite filling, (b) fracture bifurcation and bitumen filling, (c) conjugate fracture networks, (d) one conjugate fracture set offsets another, with calcite cementation, (e) conjugate fractures terminate with an open void, microfractures are developed in the confluent intersection, (f) conjugate fractures offset each other.

(2015) studied conjugate fault dihedral angles in the Canyon Range, USA, where the average angle was 59°. Those faults developed at around 10 km depth, with much greater confining pressures than the shallow-developed Halahatang Ordovician faults. This is in keeping with the positive correlation between confining pressure and dihedral angle outlined above. There is also far less dihedral angle scatter in the Halahatang area than in the Canyon Range (Ismat, 2015). Notably the dihedral angles of the conjugate faults do not increase as fault depth increases from the northern to the southern Halahatang area. This may be explained by the formation of a stable and consistent carbonate platform during the Middle to Late Ordovician (Du Jinhu, 2010; Wu Guanghui et al., 2016), resulting in only a modest thickness change in the broader slope of the platform in which the pure shear faults developed. Hence no clear positive correlation between confining pressure and conjugate fault dihedral angle is evident in the Ordovician carbonates of the Halahatang area.

The Cambrian carbonates are over 2000 m deeper than the top of the Ordovician carbonates and the distribution of major faults within these can be distinguished using structural mapping and seismic attributes (Fig. 3). Regardless of lower resolution, the conjugate fault dihedral angles in the Cambrian strata are broadly consistent with those of the Ordovician (Fig. 6c). Confining pressure, controlled by depth, may exert more influence on dihedral angles in strong extensional or compressional settings, as fault dip tends to decrease with depth (Ferril et al., 2009; Morley, 2014). However, in the strike-slip fault zones of the Halahatang area, fault dip generally increases with depth until sub-vertical. This suggests less confining pressure on the fault surface as its depth increases. Accordingly, the conjugate fault sets show no relationship between their dihedral angle and depth, implying that confining pressure is not the dominant control on conjugate fault dihedral angles in the Halahatang area.

Lithology, folding, fault reactivation and localized stress fields are all possible influences on the scatter of conjugate fault dihedral angles (e.g., Mandl, 2000; Ismat, 2015). Lithologies with a higher cohesive strength generally produce greater dihedral angles (Ismat, 2015). However, in the large inner platform, the tight limestones of the Ordovician have a relatively consistent lithology and cohesive strength (Du Jinhu, 2010). This suggests lithology can only have been a minor influence on the observed dihedral angle scatter. Similarly, folding in the Halahatang area is only weak, so probably exerts little influence on dihedral angles - although it may be important in some horsts within overlapping fault zones. Dihedral angles may have been modified, in accordance with the overall shortening direction at the time, by conjugate fault reactivation during multiple stages of fault activity (Fig. 4 and 5) (Sun Dong et al., 2015; Wu Guanghui et al., 2016). This is particularly true of faults formed only shortly prior to reactivation. It is noteworthy that the conjugate fault dihedral angles have a strong negative relationship with the NW trending faults (Fig. 6c), which are the better developed member of the conjugate fault pair. Although displacement varies along these faults (Fig. 5b) this still suggests that the better developed (i.e. more active) faults exerted a greater influence upon the associated dihedral angles. The asymmetry of a conjugate fault's development not only deviates according to the maximum stress direction, but is also affected by localized stress distribution. Since there is a well-developed rhombic fault system in the Halahatang area, which despite multiple phases of faulting lacks significant asymmetry, localized stress fields are not considered a significant influence on the scatter of dihedral angles.

Maximum shortening directions may be calculated from the acute bisectors of conjugate-faults. However such a method may not be accurate if the dihedral angles are unusually large or small, as would be the case in particularly shallow or deep faulting (Ismat, 2015). Neither can it be relied upon in cases where variations in confining pressure have imposed a significant variation upon conjugate fault dihedral angles. Figure 10 plots dihedral angles from the top of the Ordovician strata against maximum stress direction, determined from the acute bisectors of those angles. These data show a variation in maximum shortening direction of up to 18° (Table 2). However, except for a few scattered data relating to irregular and/or reactivated faults, the maximum stress directions are mostly in a narrow range from -0.8° to 6.1°, with a mean of 2.4°. Importantly we note that as the strike of the Ordovician faults deviates away from the N-S axis, the associated dihedral angle tends to increase. The result is that a relatively consistent maximum compression direction is determined from the acute bisector, despite fault strike variations. Moreover, this maximum compression direction is consistent with the regional stress field documented for the late Ordovician (Jia Chengzao, 1997; He Zhiliang et al., 2015; Wu Guanghui et al., 2016). Thus, the intersection angles of the conjugate faults can be used to determine the direction of maximum shortening in the Halahatang area, as confining pressure has not significantly affected dihedral angles.

### 5.2 The intersection of conjugate strike-slip faults

The mechanics of convergence are the major constraint

**Table 2 The maximum stress direction vs. dihedral angle at the top of the Ordovician carbonates**

| dihedral angle (°) | maximum stress direction (°) | dihedral angle (°) | maximum stress direction (°) | dihedral angle (°) | maximum stress direction (°) |
|---|---|---|---|---|---|
| 29.2 | −5.5 | 32.9 | 1.05 | 41.5 | 3.75 |
| 48 | −3.9 | 51.1 | 1.05 | 41 | 4.8 |
| 30.6 | −3.9 | 42.2 | 1.2 | 45.3 | 5.05 |
| 43.8 | −0.8 | 37.9 | 1.35 | 41.4 | 5.5 |
| 39.4 | −0.7 | 46.6 | 1.5 | 39.1 | 5.55 |
| 33.6 | −0.6 | 42.8 | 1.9 | 39.8 | 5.9 |
| 35.8 | 0.1 | 45.5 | 2.05 | 33.2 | 6.1 |
| 39 | 0.4 | 41.1 | 2.15 | 43 | 7.3 |
| 40.3 | 0.45 | 41.4 | 2.8 | 34.2 | 10.7 |
| 48.7 | 0.55 | 43.2 | 3.4 | 26.3 | 12.25 |

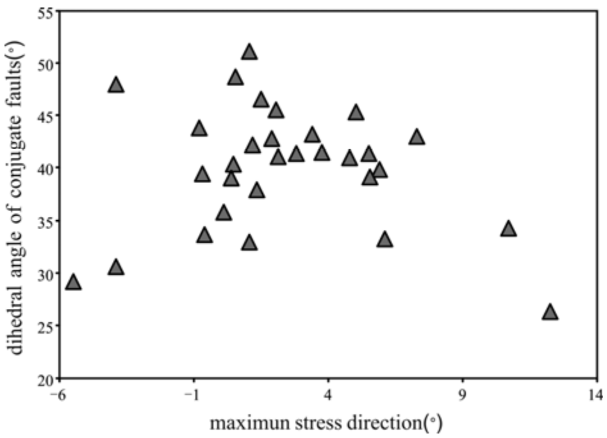


Fig. 10. The maximum stress direction vs. the dihedral angle of conjugate faults at the top of the Ordovician carbonates.

in the development of conjugate faults (Thatcher and Hill, 1991; Bretan et al., 1996; Ferrill, et al., 2009; Morley, 2014). Generally converging conjugate faults are thought to intersect and cross-cut in complicated ways that may result in volume loss (Nicol et al., 1995; Ferrill et al., 2009; Morley, 2014). Synchronous movement of conjugate faults is possible under certain conditions (Nicol et al., 1995). However, more often, complicated faults intersect and mutually offset each other in a sequential manner, within the intersection region (e.g., Ferrill et al., 2009). Differences in length or orientation relative to the principal strain axis between two faults of a conjugate pair may lead to one fault offsetting the other (e.g., Ferrill et al., 2009; Morley, 2014; Ismat, 2015). Even during synchronous conjugate fault development high strain areas in the intersection area may cause volume loss through pressure solution (Nicol et al., 1995; Kelly, 1998), particularly in carbonate rocks.

On a microscopic scale, conjugate fractures are common in the Ordovician carbonate rocks of the Halahatang area (Fig. 9). Most often these conjugate fractures cross-cut each other, or are cross-cut by another fracture, forming a pattern of alternating displacement. In the examined cores and thin sections one set of fractures is preferentially developed, even when both faults of the conjugate pair fractured synchronously. Furthermore, one set of fractures is often terminated or confined by another conjugate fracture. Simultaneous displacement of conjugate fractures is rare, although it may have occurred in a few of the thin sections examined. It is well established that microstructures may reveal useful information about larger scale fault deformation with which they are associated (Vermilye and Scholz, 1998; Janssen et al., 2016). The microstructures in the Ordovician carbonates suggest that the associated larger scale conjugate faults of the Halahatang area might have initiated as simultaneous conjugate joints (Fig. 11b). However synchronous fault displacement is rare, particularly as a large displacement in a competent conjugate fault zone (e.g. Ferrill et al., 2009; Morley, 2014). Consequently, the convergent conjugate faults may have been accommodated by alternating cross-cutting within the intersection zone.

Fault intersection relationships in the Halahatang area were identified using high resolution seismic data (Fig. 5b) (Sun Dong et al., 2015; Wu Guanghui et al., 2016). This is despite the fact that imaging of conjugate faults using seismic data is generally considered to be problematic (Bretan et al., 1991; Morley, 2014). Our structural mapping indicates that some of the NE striking faults developed upward into the Mesozoic (Figs. 4 and 5). By contrast the NW striking faults terminate in the Ordovician (Fig. 5b). In plan view (Figs. 2 and 3) the offset of NW striking faults by NE striking faults is difficult to accurately determine. This ambiguity may indicate cross-cutting by late fault activity or a synchronous faulting event. The clustered dihedral angles and relatively well preserved rhombic fault grids within the Halahatang area probably indicate a simultaneous displacement of the conjugate faults. The NE striking faults generally have smaller displacements (Fig. 8b) and some of them are truncated by the NW striking faults (Fig. 2). Thus, at a relatively early stage, the NW striking faults were the dominant fault and cut across the NE striking faults (Fig. 11c). The relative lack of complexity within the intersections of the conjugate pairs supports sequential

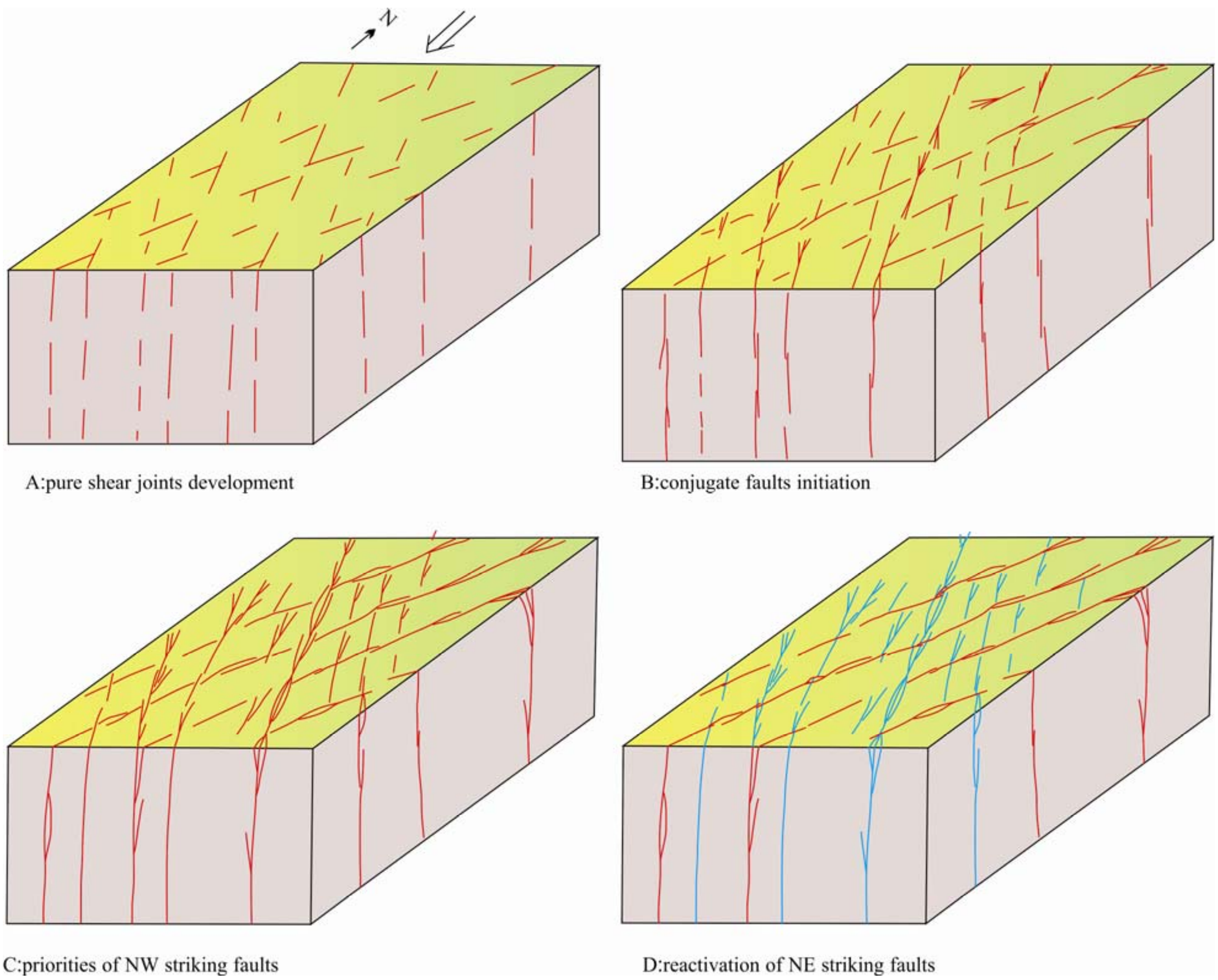


Fig. 11. The conjugate fault evolution and intersection in the Ordovician carbonate in Halahatang area. The blue traces indicate dormant faults.

rather than simultaneous slip on the constituent faults (Nicol et al., 1995; Ferrill et al., 2009). Sequential faulting also resolves the apparent geometric space problem in the intersection regions and, in conjunction with the development of dominant NW striking faults, increases the likelihood of preserving an undistorted rhombic form within the fault system (e.g., Ferrill et al., 2009).

Volume balance and strain compatibility are critical and interdependent issues within conjugate fault intersection regions (e.g., Bretan et al., 1996; Ferrill et al., 2009; Morley, 2014). With this in mind it is worth noting that the Ordivician fault zone lengths are up to 70 km, whilst their maximum throw is less than 140 m (Fig. 8a). Although discriminating horizontal separation at the top the Ordovician carbonate is problematic, previous studies suggest there is relatively little displacement across the broader slope (Sun Dong et al., 2015; Wu Guanghui et al., 2016). Where there is higher displacement it is mostly focused around overlapping fault zones (Figs. 4 and 5). The significance of a relatively small displacement is that there is less likely to be a space problem within the associated fault intersection. In addition the observed development of many short axis folds, generally small low relief antiforms, may accommodate contraction within the intersections. Furthermore, in core and thin section abundant stylolites were observed in the Ordovician limestones (Fig. 9), indicating intense pressure solution (Du Jinhu, 2010; Ni Xinfeng et al., 2013) focused within the intersection regions. Volume loss resulting from pressure solution is known to be an effective means of accommodating strain within intersection regions (e.g., Morley, 2014).

The heterogenous growth of the conjugate faults gradually prioritized the growth of NW striking faults (Figs. 2 and 11c). Consequently, the NW striking faults are more abundant and longer than those striking NE, although NE striking faults were more often subjected to later reactivation. From that point onwards the conjugate fault system began evolving asymmetrically, developing much more variation between the two fault sets. This would have aided strain and displacement balance in the Halahatang area. However, some NE trending strike-slip faults reactivated in the Permian and Mesozoic (Figs. 4 and 5) (Wu Guanghui et al., 2016). A series of *en echelon* fault zones occurred in the Mesozoic (Sun Dong et al., 2015; Wu Guanghui et al., 2016), forming micro-grabens. These densely spaced *en echelon* faults are right-stepping and merge downwards to the Ordovician carbonates. Strong transtensional faulting was concentrated in the Mesozoic, in contrast to the weak deformation of the Ordovician (Figs. 4 and 5). Consequently, the dominant NW striking faults are cut across by small reactivated NE striking faults (Fig. 11d), although their offset is unclear (Sun Dong et al., 2015; Wu Guanghui et al., 2016).

In summary, the intersection of the conjugate faults initially resulted from sequential slip of the cross-cutting conjugate faults. Then a stage of greater displacement came on the NW striking faults. Finally, the NE striking faults were reactivated, cutting across the NW striking faults (Fig. 11). The fractures, folds and pressure solution associated with these faults may have played an important role in the development of the conjugate fault intersections and were important in maintaining volume balance. Despite “X” shaped conjugate fault systems not usually being evident in intracratonic basins, the conjugate strike-slip fault system is both well developed and preserved in the Halahatang area.

## 6 Conclusions

(1) A large conjugate strike-slip fault system developed within the broader slope of the Tarim Basin, consisting of faults up to 70 km long but with less than 140 m vertical throw. The best developed rhombic conjugate fault geometries occur within Cambrian to Ordovician carbonates. Partial reactivations of these faults during the Permian to Mesozoic, associated with both transpression and transtension, have superimposed a complicated layered architecture upon the earlier faults. At the microstructural scale, conjugate fractures were observed in cores and thin sections associated with the larger conjugate faults.

(2) The dihedral angles of the conjugate faults have a narrow range of 26° to 51° with a mode of ~44° in the Ordovician, and a range of 19° to 62° with a mode of ~42° in the Cambrian. This is markedly different from the ~60° predicted by the Coulomb fracture criterion. The dihedral angles show a good correlation with the strike of the NW trending faults, but much weaker correlation with the NE trending faults. This suggests a preferential relationship between the dihedral angle values and the NW trending faults.

(3) The dihedral angles of the conjugate fault systems formed at shallow depths within a buried late Ordovician carbonate platform. These angles did not vary with depth, suggesting confining pressure did not exert a clear control over dihedral angle values. Fault reactivation and localized stress fields may have influenced the scatter of dihedral angles. Maximum shortening directions of −0.8° to 6.1° were determined from the intersection angles of conjugate faults at the top of the Ordovician carbonates. Importantly these directions are consistent with the published shortening direction for the Tarim Basin during the late Ordovician.

(4) The displacement balance within conjugate fault intersections was likely maintained by sequential movement of the two constituent faults. Furthermore fractures, folds and pressure solution associated with the conjugate faults may have played an important role in maintaining volume balance and therefore the development of the conjugate fault geometries within the fault intersections. The conjugate fault system probably started with mutual fracturing of rhombic pure shear joints within a broad platform. From this evolved "X" type conjugate fault segments. Then the NW striking faults became dominant, before later reactivation of NE striking faults that cut across the NW striking faults.

## Acknowledgments

The authors thank the Tarim Oil Company for data support and project research. We are grateful to Zhang Lijuan, Li Guohui, Ma Debo and Luo Haoyu for their help. Comments provided by editors and reviewers of the manuscript are much appreciated and were very helpful in improving the paper. This study has been partly supported by National Natural Science Foundation of China (Grant No. 41472103).

Manuscript received Jan. 1, 2017
accepted Aug. 10, 2017
edited by Liu Lian

**References**

Aktar, M., Karabulut, H., Özalaybey, S., and Childs, D., 2007. A conjugate strike‑slip fault system within the extensional tectonics of Western Turkey. *Geophysical Journal International*, 171(3): 1363–1375.

Bretan, P.G., Nicol,A., and Walsh, J.J., 1996. Origin of some conjugate or "X" fault structures. *The Leading Edge*, 15(7): 812–816.

Cui Haifeng, Zheng Duoming and Teng Tuanyu, 2009. Petroleum geologic characteristics and exploration orientation in Halahatang Depression of Tabei uplift. *Lithological Reservoir*, 21(2): 54–59 (in Chinese with English abstract).

Davatzes, N.C., and Aydin, A., 2003. The formation of conjugate normal fault systems in folded sandstone by sequential jointing and shearing, Waterpocket monocline, Utah. *Journal of Geophysical Research*, 25: 1795–1813.

Dooley, T.P., and Schreurs, G., 2012. Analogue modelling of intraplate strike-slip tectonics: A review and new experimental results. *Tectonophysics*, 574–575: 1–71.

Du Jinhu, 2010. *Oil and gas exploration of Cambrian-Ordovician carbonate in Tarim Basin*. Beijing: Petroleum Industry Press (in Chinese).

Ferrill, D.A., Morris, A.P., and McGinnis, R.N., 2009. Crossing conjugate normal faults in field exposures and seismic data. *AAPG Bulletin*, 93(11): 1471–1488.

Freund, R., 1974. Kinematics of transform and transcurrent faults. *Tectonophysics*, 21(1): 93–134.

Harding, T.P., 1990. Identification of wrench fault using subsurface structural data: criteria and pitfalls. *American Association of Petroleum Geologists Bulletin*, 74(10): 1090–1609.

He Zhiliang, Gao Shanlin and Zheng Menglin, 2015. Regional tectonic framework and evolution of superimposed basins in northwestern China. *Earth Science Frontiers*, 22(3): 227–240 (in Chinese with English abstract).

Horsfield, W.T., 1980. Contemporaneous movement along crossing conjugate normal faults. *Jounral of Structral Geology*, 2(3): 305–310.

Ismat, Z., 2015. What can the dihedral angle of conjugate-faults tell us? *Jounral of Structral Geology*, 73: 97–113.

Janssen, C., Wenk, H.-R., Wirth, R., Morales, L., Kemnitz, H., Sulem, G., and Dresen, J., 2016. Microstructures and their implications for faulting processes –Insights from DGLab core samples from the Gulf of Corinth. *Journal of Structural Geology*, 86: 62–74.

Jia Chengzao, 1997. *Tectonic characteristics and petroleum, Tarim basin, China*. Beijing: Geological Publishing House, 29–261 (in Chinese)

Jiang Haijian, Chen Qianglu, Yang Xing and Chu Chenglin, 2017. The Style of Sequence Stratigraphy of Neoproterozoic Rift Basin in the Tarim Basin. *Acta Geologica Sinica*, 91(3): 588–604 (in Chinese with English abstract).

Jin Zhijun, Zhu Dongya, Hu Wenxuan, Zhang Xuefeng, Zhang Juntao and Song Yucai, 2009. Mesogenetic dissolution of the middle Ordovician limestone in the Tahe oilfield of Tarim basin, NW China. *Marine and Petroleum Geology*, 26(6): 753–763.

Kang Yuzhu, 2007. Review and revelation of oil/gas discoveries in the Paleozoic marine strata of China. *Oil & Gas Geology*, 28(5): 570–576 (in Chinese with English abstract).

Kelly, P.G., Sanderson, D.J., and Peacock, D.C.P., 1998. Linkage and evolution of conjugate strike-slip fault zones in limestones of Somerset and Northumbria. *Jounral of Structral Geology*, 20: 1477–1493.

Lan Xiaodong, LüXiuxiang, Zhu Yanming and Yu Hongfeng, 2015. The geometry and origin of strike-slip faults cutting the Tazhong low rise megaanticline (central uplift, Tarim Basin, China) and their control on hydrocarbon distribution in carbonate reservoirs. *Journal of Natural Gas Science and Engineering*, 22: 633–645.

Leighton, M.W., Kolata, D.R., Oltz, D.F., and Eidel, J.J., 1990. *Interior cratonic basins*. American Association of Petroleum Geologists.

Li Qiming, Wu Guanghui, Pang Xiongqi, Pan Wenqing, Luo Chunshu, Wang Chenglin, Li Xinsheng and Zhou Bo, 2010. Hydrocarbon accumulation conditions of Ordovician carbonate in Tarim Basin. *Acta Geologica Sinica* (English Edition), 84(5): 1180–1194.

Mandl, G., 2000. *Faulting in Brittle Rocks: an Introduction to the Mechanics of Tectonic Faults*. Springer, New York.

Morley, C.K., 2014. Outcrop examples of soft-sediment deformation associated with normal fault terminations in deepwater, Eocene turbidites: A previously undescribed conjugate fault termination style? *Jounral of Structral Geology*, 69: 189–208.

Ni Xinfeng, Shen Anjiang, Pan Wenqing, Zhang Ronghu, Yu Hongfeng, Dong Yong, Zhu Yongfeng and Wang Caofeng, 2013. Geological modeling of excellent fracture-vug carbonate reservoirs: a case study of the Ordovician in the northern slope of Tazhong palaeo-uplift and the southern area of Tabei slope, Tarim Basin, NW China. *Petroleum Exploration and Development*, 40(4): 444–453.

Nicol, A., Walsh, J.J., Watterson, J., and Bretan, P.G., 1995. Three dimensional geometry and growth of conjugate normal faults. *Jounral of Structral Geology*, 17: 847–862.

Nixon, C.W., Sanderson, D.J., and Bull, J.M., 2011. Deformation within a strike-slip fault network at Westward Ho!, Devon U.K.: Domino vs conjugate faulting. *Jounral of Structral Geology*, 33: 833–843.

Pang Xiongqi, Tian Jun, Pang Hong, Xiang Caifu, Jiang Zhenxue and Li Sumei, 2010. Main progress and problems in research on Ordovician hydrocarbon accumulation in the Tarim Basin. *Petroleum Science*, 7(2): 147–163.

Peng Gengxin, Dan Guangjian, Zheng Duoming, Li Haiyin, Gao Lianhua and Yang Pengfei, 2011. 3D prestack depth migration quantitative characterization of carbonate reservoirs in Halahatang area, Tarim basin. *Petroleum Exploration and Development*, 5(z1):49–56 (in Chinese with English abstract).

Ramsey, J.M., and Chester, F.M., 2004. Hybrid fracture and the transition from extension fracture to shear fracture. *Nature*, 428(6978), 63–66.

Schwarz, H.U., and Kilfitt, F.W., 2008. Confluence and intersection of interacting conjugate faults: A new concept based on analogue experiments. *Jounral of Structral Geology*, 30: 1126–1137.

Sun Dong, Yang Lisa, Wang Hongbin, Zheng Duoming, Sun Qinhua, Li Guohui, Dai Dongdong and Fang Qifei, 2015. Strike-slip fault system in Halahatang area of Tarim Basin and its control on reservoirs of Ordovician marine carbonate rock. *Natural Gas Geoscience*, 26(S1): 80–87(in Chinese with English abstract).

Sylvester, A.G., 1988. Strike-slip faults. *Geological Society of America Bulletin*, 100: 1666–1703.

Thatcher, W., and Hill, D.P., 1991. Fault orientations in extensional and conjugate strike-slip environments and their implications. *Geology*, 19(19): 1116–1120.

Vermilye, J.M., and Scholz, C.H., 1998. The process zone: a microstructural view. *Journal of Geophysical Research*, 103: 12223–12237.

Walker, R., and Jackson, J., 2002. Offset and evolution of the Gowk fault, S.E. Iran: a major intra-continental strike-slip system. *Jounral of Structral Geology*, 24: 1677–1698.

Wang Hui and Liu Mian, 2013. Evolution from step-overs to bends on strike-slip faults: primary results. *Acta Geologica Sinica* (English Edition), 87(z1): 1916–1919.

Wang Zhe and Wang Xin, 2016. Late Cenozoic Deformation Sequence of a Thrust System along the Eastern Margin of Pamir, Northwest China. *Acta Geologica Sinica* (English Edition), 90(5): 1664–1678.

Wu Guanghui, Yang Haijun, Qu Tailai, Li Honghui and Luo Chunshu, 2012. The fault system characteristics and its controlling roles on marine carbonate hydrocarbon in the Central uplift, Tarim Basin. *Acta Petrologica Sinica*, 28(3): 793–805 (in Chinese with English abstract).

Wu Guanghui, Pang Xiongqi, Li Qiming and Yang Haijun, 2016. *The structural characteristics of carbonate rocks and their effects on hydrocarbon exploration in craton basin: A case study of the Tarim Basin*. Beijing: Science Publishing House (in Chinese).

Wu Zhenhan, Zhao Zhen, Barosh, P.J., and Ye Peisheng, 2016. Early Cretaceous tectonics and evolution of the Tibetan Plateau. *Acta Geologica Sinica* (English Edition), 90(3): 847–857.

Yin, A., and Taylor, M., 2011. Mechanics of V-shaped conjugate strike-slip faults and the corresponding continuum mode of continental deformation. *Bulletin of the Geological Society of America*, 123 (9-10): 1798–1821.

Zhao Guozhu and Johnson, A.M., 1991. Sequential and incremental formation of conjugate sets of faults. *Geological Society London, Special Publications*, 13(8): 887–895.

Zhao Kuanzhi, Zhang Lijuan, Zheng Duoming, Sun Chonghao and Dang Qingning, 2015. A reserve calculation method for fracture-cavity carbonate reservoirs in Tarim Basin, NW China. *Petroleum Exploration and Development*, 42(2): 277–282.

Zhu Guangyou, Zhang Shuichang, Su Jin, Zhang Bin, Yang Haijun, Zhu Yongfeng and Gu Lijing, 2013. Alteration and multi-stage accumulation of oil and gas in the Ordovician of the Tabei Uplift, Tarim Basin, NW China: Implications for genetic origin of the diverse hydrocarbons. *Marine and Petroleum Geology*, 46(4): 234–250.

## About the first author

WU Guanghui, male, born in 1971, Ph.D. He is now an associate professor at School of Marine Sciences, Sun Yat-sen University, and is mainly engaged in structural geology and petroleum geology researches. E-mail: wuguangh@mail.sysu.edu.cn.